ELSEVIER International Journal of Mass Spectrometry and Ion Processes 149/150 (1995) 373–387

On the dynamics of the reaction of positive hydrogen cluster ions (H_5^+ to H_{23}^+) with para and normal hydrogen at 10 K☆

W. Paul, B. Lücke, S. Schlemmer, D. Gerlich*

Department of Physics, Technical University Chemnitz-Zwickau, D-09107 Chemnitz, Germany

Received 20 May 1995; accepted 24 June 1995

Abstract

The dynamics of clustering and fragmentation reactions $H_i^+ + 2H_2 \rightleftharpoons H_{i+2}^+ + H_2$, for odd i, was studied at a nominal temperature of 10 K in a 22-pole radio-frequency ion trap in normal hydrogen and para-enriched hydrogen. Ternary association rate coefficients, k_3, and binary fragmentation rate coefficients, k_f, were extracted from the measured temporal evolution of the hydrogen cluster ion intensity, $I(H_i^+)$, for $i = 3, \cdots, 23$. Pure para hydrogen enhances the rate coefficients for association and fragmentation. For $i > 9$ this general trend is explained by a difference in the capture cross-sections, k_c, for the two hydrogen nuclear spin modifications. Significant differences in k_3 which remain for small clusters ($i < 9$) are due to the availability of the $J = 1$ rotational energy of the ortho modification when merging into the cluster. This surprising result is discussed in the framework of simple dynamical and energetic considerations. Possible structures of the cluster can be classified and estimates for the bond energy of the outermost H_2 in the cluster as a function of cluster size are derived.

Keywords: Cluster fragmentation; Cluster growth; Ionic hydrogen clusters; Low temperature ion/molecule reaction; Reaction dynamics

1. Introduction

The smallest positive hydrogen cluster ion, H_5^+, was identified in 1962 by Dawson and Tickner [1]. Since then much experimental [2–4] and theoretical work [5–8] has been stimulated by the interesting properties of this simple cluster ion system. Mass spectra are dominated by odd mass hydrogen clusters [4,9]. Binding energies ranging from several kcal mol^{-1} for the H_5^+ system to the heat of evaporation (approx. 0.2 kcal mol^{-1}) of liquid hydrogen indicate a transition from a chemically bound molecular ion to a van der Waals bound cluster.

Regarding the dynamics of the growth and fragmentation of hydrogen cluster ions the two independent nuclear spin species, para (even J) and ortho (odd J) hydrogen, have to be considered for several reasons. Nuclear spin symmetry restrictions for identical particles as well as the difference in rotational energy may cause interesting changes in reaction probability and other features of the clusters depending

☆ Dedicated to Professor David Smith FRS on the occasion of his 60th birthday.

* Corresponding author.

SSDI 0168-1176(95)04269-5

on the nuclear spin state of the reactants (target molecule and cluster).

Theoretical work has focused on the structure, binding energies, and spectroscopic properties of hydrogen cluster ions [5,7,8,10–12]. Ab initio calculations have been carried out at Hartree–Fock (SCF) and configuration interaction (CI, CISD) level of theory in order to predict equilibrium geometries, vibrational frequencies, infrared intensities and binding energies. Basis sets have been improved from double zeta (DZ) [11] to triple zeta plus polarization (TZP) [12] over the years. Fully optimized structures and bond energies of H_{11}^+ and H_{13}^+ support the shell model in which larger clusters ($H_i^+, i \geq 11$) consist of an H_9^+ core with attached H_2 molecules [12]. For larger clusters the potential energy surface becomes very shallow. Therefore, depending on the internal energy, many different low lying stationary points of the potential energy surface (PES) are accessible to the cluster.

A significant part of the experimental work on hydrogen cluster ions has concentrated on the properties at thermodynamic equilibrium [4,13–16]. Steps in the dissociation enthalpies indicate a shell structure with closed shell configurations at cluster sizes H_9^+ and H_{15}^+ [4,13].

Interesting spectroscopic information was obtained by Okumura et al. [17] who studied vibrational predissociation of clusters up to H_9^+. The low resolution bands of the solvent H_2 stretch vibrations near 4000 cm^{-1} show a red shift that supports the model of H_9^+ as an H_3^+ with a complete solvation shell of three H_2 molecules.

Concerning the fragmentation of ionic hydrogen clusters there have been several experiments at collision energies in the kiloelectronvolt range with different targets [18–21]. These investigations reveal information on the dynamical stability of the fragmentation products. Recent experiments have been performed in a megaelectronvolt cluster accelerator.

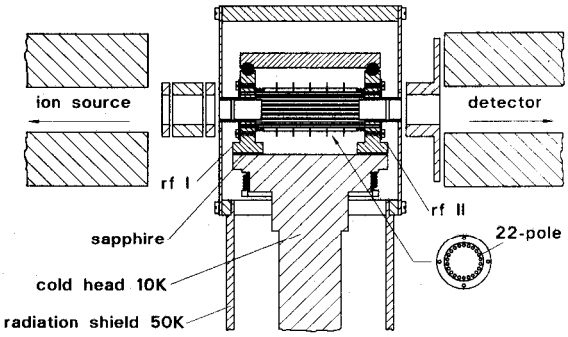

Fig. 1. Experimental setup: this section of the ion trap apparatus depicts the cryocooled 22-pole r.f. ion trap (10 K). Mass-selected ions from the ion source are stored in the trap for selected periods of time and the products are mass analyzed thereafter and detected.

The resulting interaction times in the femtosecond range give rise to interesting multifragmentation processes [22]. To our knowledge the present study is the first investigation of the dynamics of the fragmentation process at collision energies comparable to the binding energies of the clusters.

Studies of the dynamics of the cluster ion growth have been restricted to the formation of the smallest cluster, H_5^+. Ternary association rate coefficients of the reaction $H_3^+ + 2H_2 \rightarrow H_5^+ + H_2$ have been determined at temperatures down to 80 K [13,23–25]. In this paper we present the first measurements of rate coefficients for ternary association of ionic hydrogen clusters up to H_{21}^+.

2. Experimental

The growth and fragmentation of hydrogen cluster ions are studied in a variable-temperature 22-pole radio-frequency (r.f.) ion trap (10–300 K). The trap, which will be described in detail below, is part of an ion beam apparatus. In the present experimental setup (see Fig. 1) primary ions are created from hydrogen gas, mass selected in a quadrupole mass filter and injected into the ion trap, where reaction with hydrogen gas is taking place. After a

given reaction time (typically 5 ms–5 s) primary and product ions are extracted from the trap, mass analyzed in a second quadrupole mass filter and detected by single ion counting. For a thorough description of the guided ion beam technique and r.f. trapping devices the reader is referred to Refs. [26,27].

2.1. The 22-pole ion trap

Ions in a high order r.f. multipole trap are confined by an effective potential that is characterized by a wide field-free region bounded by steep walls. Our trap consists of 22 stainless steel rods with a diameter of 1 mm and a length of 36 mm equally spaced on an inscribed radius $r_0 = 5$ mm. The whole unit is housed in a copper box which is mounted on the second stage of a closed cycle cryocooler (Leybold RGD 210) capable of 2 W of cooling power at 20 K; the lowest achievable temperature is slightly below 10 K. Sheets of sapphire, 0.5 mm thick, covered with a foil of indium for close contact, serve as electrical insulator, as well as an excellent heat bridge. The surrounding radiation shield is in thermal contact with the first cooling stage at a temperature of approximately 50 K. All connections and gas lines are precooled to that temperature before they enter the copper box. The target gas pressure in the trap is measured using a spinning rotor gauge (MKS) operating at room temperature. The indicated pressure p (mbar) is converted into a number density n using the relation

$$n = 4.19 \times 10^{17} p T^{-1/2} \text{ cm}^{-3}$$

where T is the trap temperature in kelvins. Corrections for thermal transpiration [28] can be neglected, because in the present setup wall collisions inside the gas line are more frequent than gas kinetic collisions. However, several other error sources for the determination of n have to be considered. Possible errors are caused by the inaccuracy of the pressure gauge (quoted accuracy 5%), uncertainties of the actual gas temperature, and a density gradient along the trap axis. At the low temperatures of our experiment, small temperature variations can cause significant density fluctuations due to condensation and evaporation of the hydrogen target gas. Therefore our conservative estimate of the resulting error for n is 50%.

The effective collision temperature of the ion/molecule interaction, T_{coll}, is the mass-weighted average of the temperature of the target gas, T_B, which is essentially the temperature of the copper box and the "temperature" of the ions, T_{A^+}:

$$T_{\text{coll}} = (m_{A^+} T_B + m_B T_{A^+})/(m_{A^+} + m_B)$$

The temperature of the ions is coupled to the temperature of the target gas via inelastic collisions. Under typical conditions ($n = 5 \times 10^{13}$ cm^{-3}) collisions occur at a frequency of about 10^4 s^{-1}; therefore the ion temperature reaches the ambient gas temperature after a time interval on the order of milliseconds.

Despite this effective cooling mechanism, ions remain at a slightly elevated temperature due to modulation of their kinetic energy by the r.f. field at the boundary of the trap. The effective ion temperature above 50 K in the 22-pole trap has been determined by spectroscopic methods [29]. Below 50 K the collision temperature has been measured with the help of temperature-dependent rate coefficients [30]. We find good overall agreement of these temperatures over the whole accessible temperature range. At present the ion temperature at the lowest achievable cold head temperature ($T_B = 10$ K) is 15 ± 5 K.

Purified hydrogen (99.999%) is used as target gas. In some of the experiments the para hydrogen content of the target gas was varied using a catalytic para hydrogen generator at temperatures between 15 K and room

temperature to yield a concentration in the range of 25–100%. The content was calculated from the temperature of the catalyst under the assumption of complete thermalization. The error in this temperature is estimated to be smaller than 5 K, corresponding to a maximum error of 15% in para hydrogen content.

Experiments have been performed using two different ion sources. In the storage ion source, which has been described earlier [27], primary ions are produced by electron bombardment of hydrogen gas. H_3^+ is formed efficiently in subsequent collisions of H_2^+ ions with the source gas (H_2). Most of the ions are cooled to the ambient source temperature of 400 K by 100–1000 gas collisions before they leave the source through a pulsed electrode. In order to inject hydrogen cluster ions larger than H_3^+ into the trap we built a corona discharge source.

2.2. Corona discharge source

The source is similar to the type described by Beuhler et al. [14]. Cryocooling of the source and the hydrodynamic expansion of the partly ionized gas is utilized to produce cold large cluster ions. The body of the corona discharge source is made from stainless steel. The sharpened tip of a thin ($d = 0.3$ mm) rhenium wire is mounted at a distance of about 1 mm from the nozzle orifice with a diameter of 30 μm. A positive point corona discharge is struck from the wire tip to the source body. The source chamber is separated from the chamber of the first quadrupole by a steel plate with a 5 mm hole. Nozzle and steel plate are electrically insulated and can be floated with respect to ground potential. The source is attached to the second stage of a closed cycle cryocooler capable of 20 W of cooling power at a temperature of 50 K via a thick braided copper wire. Electrical insulation from the cryocooler is achieved by a sheet of sapphire. In this setup the nozzle reaches a lowest temperature of approximately 60 K. As source gas we use high purity hydrogen (Messer-Griesheim, 99.999%) that is further purified by a molecular sieve at liquid nitrogen temperature. We operate the source at a stagnation pressure of 100 Torr to limit the gas load of the trapping region. Under these conditions the corresponding background pressure in the trap is below 3×10^{-6} Torr (or $n = 4.2 \times 10^{11}$ cm^{-3}). At room temperature this source produces an ion current that corresponds to a continuous beam intensity of 3×10^6 H_5^+ ions s^{-1} transmitted to the detector. Typical discharge parameters are 400 V and 20 μA. At the lowest achievable temperature the total ion current increases by a factor of 5 and is dispersed over a wide range of cluster sizes peaking at H_{25}^+ at a rate of 3×10^6 ions s^{-1}.

3. Results

Fig. 2 shows histograms of two representative mass spectra depicting the measured product cluster ion intensities when H_3^+ is stored in normal hydrogen (upper panel in Fig. 2) and para hydrogen (lower panel in Fig. 2) respectively. The spectra were taken after a reaction time of 9.9 s at a target gas number density of $n_{H_2} = 1.13 \times 10^{14}$ cm^{-3}. In both cases the cluster size distribution has reached equilibrium and H_{19}^+ is the predominant ion under these conditions. Each spectrum consists of distinct odd and even mass contributions which are indicated by black and gray bars, respectively. Mass peaks which are related to cluster ions H_i^+, i odd, are dominant and surprisingly show a similar size distribution, both for p-H_2 and n-H_2. This interesting finding for the equilibrium cluster size distribution will be discussed below.

Even mass contributions are predominantly due to partial deuteration in collisions of

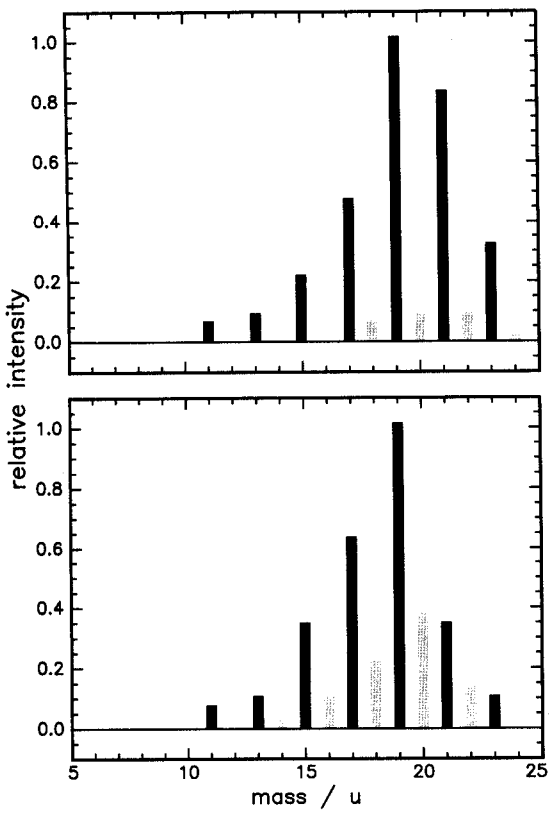

Fig. 2. Two typical mass spectra of the trap contents under equilibrium conditions. H_5^+ ions were injected into n-H_2 (upper trace) and p-H_2 (lower trace) and stored for 9.9 s at a nominal temperature of 11 K and a number density of 1.13×10^{14} cm^{-3}. Odd and even mass contributions are represented by black and gray bars, respectively. The former is the main contribution and is given by H_i^+, i odd. The latter corresponds predominantly to isotopically fractionated DH_{i-1}^+.

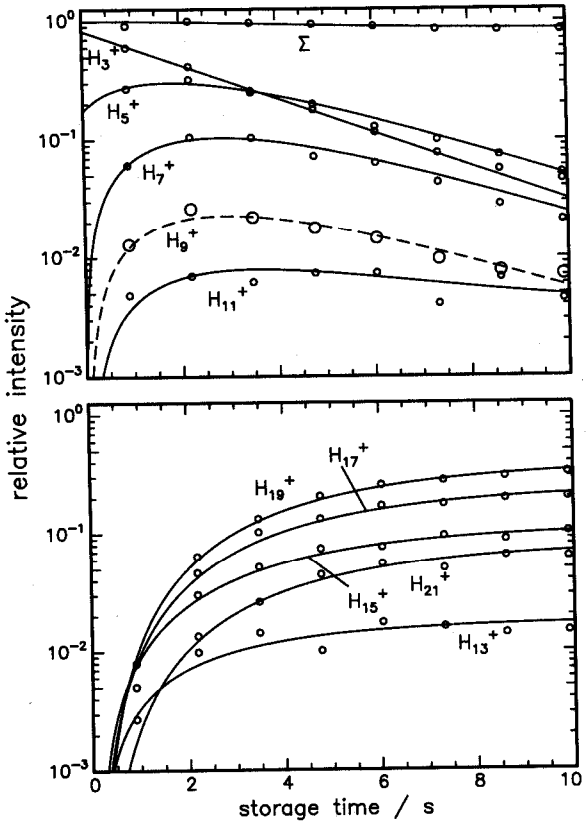

Fig. 3. Evolution of trap contents after injection of H_3^+ into n-H_2 at a number density of 6.27×10^{13} cm^{-3} and a nominal temperature of 10 K. Symbols represent experimental data points and lines best fits according to the analysis given in the text.

clusters with HD impurities. The natural abundance for D/H of 1.5×10^{-4} results in a statistical probability for finding, for example, one D in H_{19}^+ of about 0.3%. Measured fractions are much larger than this value, by about 10% in the case of n-H_2 and 30% in the case of p-H_2. This isotopic enrichment, known as isotopic fractionation, is due to different zero-point energies of the isotopes [31]. The effect is more pronounced in the case of a non-rotating target ($J = 0$), where the total energy of the ensemble is much lower. Structure and stability of these deuterated clusters appear to be similar to those of the corresponding pure hydrogen cluster ions, because the relative cluster size distributions are very similar and just shifted by the mass difference of deuterium versus hydrogen. A detailed investigation of H–D exchange in hydrogen cluster ions will be discussed in a forthcoming publication.

In order to study the formation and decay of cluster ions, intensities were recorded for at least six different storage times. Each time typically 200 primary ions were injected into the trap. The product intensities of 10–20 fillings were accumulated for each storage time and mass. Fig. 3 shows the temporal evolution of the trap contents over a period of 10 s after injection of H_3^+. Intensities are normalized to

the total number of injected primary ions. Time traces were measured for primary and product ions up to H_{23}^+. The normalized sum of all counts (indicated as Σ, see Fig. 3) serves as a check that all major reaction channels are accounted for and only minor losses due to reaction with residual gas occur.

3.1. Analysis

At target gas number densities present in our experiment only bimolecular and termolecular processes have to be considered. Therefore the formation of clusters happens via the elementary reaction steps:

$$[H_i^+] + 2[H_2] \xrightarrow{k_{3,i}} [H_{i+2}^+] + [H_2]$$
$$[H_i^+] + [H_2] \xrightarrow{k_{\mathrm{rad},i}} [H_{i+2}^+] + h\nu \quad (1)$$

Here $k_{3,i}$ denotes the rate coefficient for ternary association of the ith cluster and $k_{\mathrm{rad},i}$ denotes the binary rate coefficient for radiative association of the ith cluster. The newly formed clusters are probably slightly vibrationally excited due to the gain in binding energy, but thermalization is not accounted for in the rate equation since the new clusters undergo many (approx. 1000) thermalizing collisions before they grow again.

At the collision energies of our experiment it is safe to assume that removal of one H_2 from the cluster is the main fragmentation channel, i.e.

$$[H_i^+] + [H_2] \xrightarrow{k_{\mathrm{f},i}} [H_{i-2}^+] + 2[H_2] \quad (2)$$

Here $k_{\mathrm{f},i}$ denotes the binary rate coefficient for fragmentation of the ith cluster.

This rate equation system can be translated into a set of coupled ordinary differential equations (ODE) for the concentration of the ith cluster:

$$\frac{1}{[H_2]}\frac{d[H_i^+]}{dt} = k_{g,i-2}\cdot[H_{i-2}^+] + k_{\mathrm{f},i+2}\cdot[H_{i+2}^+] - k_{\mathrm{f},i}\cdot[H_i^+] - k_{g,i}\cdot[H_i^+] \quad (3)$$

where $k_{g,i}$ denotes the effective binary rate coefficient for growth of the ith cluster and $[H_2]$ is the number density of the target gas. At a given $[H_2]$ and temperature these rate coefficients correspond to time constants:

$$\tau_{g,f} = \frac{1}{[H_2]\cdot k_{g,f}}$$

These time constants are derived from the temporal evolution of the normalized ion intensities by means of a fitting procedure. For a given set of time constants the ODE (Eq. (3)) is solved numerically. The solution is compared to the normalized ion intensities. Starting with a reasonable guess for the initial values the deviations from the measured ion intensities are minimized by means of systematic variation of the time constants following a multidimensional minimization routine first proposed by Powell (quoted in Ref. [32]).

As an example of the described fitting procedure the solid lines in Fig. 3 represent the best fit for the evolution of initially injected H_3^+. The agreement between experimental data and the best fit is very good. Only for minor product channels of the total ion signal, such as H_{13}^+, do statistical deviations become notable. In these cases the calculated curves also serve as a guide to the eye showing the main trends in the measured data.

The derived best fit time constants are used to determine binary rate coefficients for fragmentation and growth. For the association reaction our model rate equation system accounts for the ternary (second order) and radiative (first order) channels. The effective

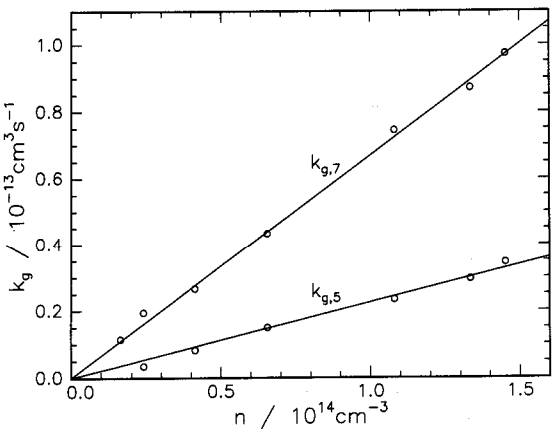

Fig. 4. Apparent binary association rate coefficient for the reaction of H_5^+ and H_7^+ with n-H_2 at 10 K as a function of the target gas number density.

binary rate coefficient k_g might therefore be written as

$$k_{g,i} = k_{rad,i} + k_{3,i} \cdot [H_2] \quad (4)$$

In Fig. 4, $k_{g,i}$ is plotted versus the target gas number density for $i = 5$ and 7, based on a series of measurements in normal hydrogen. Densities are chosen such that collisional stabilization prevails. The data points for both cluster sizes follow straight lines and ternary rate coefficients are given by the slope of these curves. To derive a value for the rate coefficient for radiative association, k_{rad}, one has to extrapolate $k_{g,i}$ down to zero target gas number density. However, in order to obtain reliable values for k_{rad}, measurements have to be extended toward lower number densities. This has not been done in the present study and therefore only an upper limit for this rate coefficient, $k_{rad} = 5 \times 10^{-15}$ cm^3 s^{-1}, can be derived from the experimental data.

The absence of systematic deviations of the measured $k_{g,i}$ from the straight line fit also shows that higher order reaction pathways are negligible, even at higher target gas densities. The experimental results also confirm the first-order character of the fragmentation process proposed in the model rate equation system (Eq. (2)). Numerical errors from the fitting procedure were much smaller than differences in the results from different measurements. More than 80% of the measurements are represented by the error bars in our plots. In summary, the quality of the fit of all our experimental data indicates that all open reaction channels are accounted for in our analysis, justifying the proposed sequential reaction model.

Using the corona discharge source, parent clusters of different sizes are injected into the trap. When starting with H_5^+ or other small clusters, growth is the dominant process and the temporal evolutions of the trap contents show very similar trends for the individual cluster sizes leading to comparable values for the associated rate coefficients. This serves as another check of the invariance of the results with respect to different initial conditions.

The use of pure p-H_2 enhances the reaction rates for all cluster sizes. A measurement of initially stored H_5^+ and its best fit using 100% p-H_2 as target gas are shown in Fig. 5. Equilibrium for this reaction is reached much faster (about 100 ms) compared to the measurement with n-H_2 (see Fig. 3) (a few seconds). Based on the assumption that rotational energy is available in collisions with o-H_2 ($j = 1 \rightarrow 0$, $\Delta E = 14.4$ meV) one might expect this behavior, but surprisingly the equilibrium cluster size distributions for reaction with p-H_2 and n-H_2 are very similar (Fig. 2). It is interesting that in the case of p-H_2 (see Fig. 5) H_9^+ temporarily appears as a dominant species (20%) compared to 2–3% in the case of n-H_2 (compare broken lines in Figs. 5 and 3). Here much more H_9^+ is formed during this time interval than is lost by further growth to H_{11}^+. Thus ternary rate coefficients for these steps ($7 \rightarrow 9$ and $9 \rightarrow 11$) will drop sharply, indicating a bottleneck in the cluster formation process at a parent cluster size of H_9^+.

When larger parent clusters are injected, fragmentation dominates at the beginning. Fig. 6 shows the temporal evolution of injected

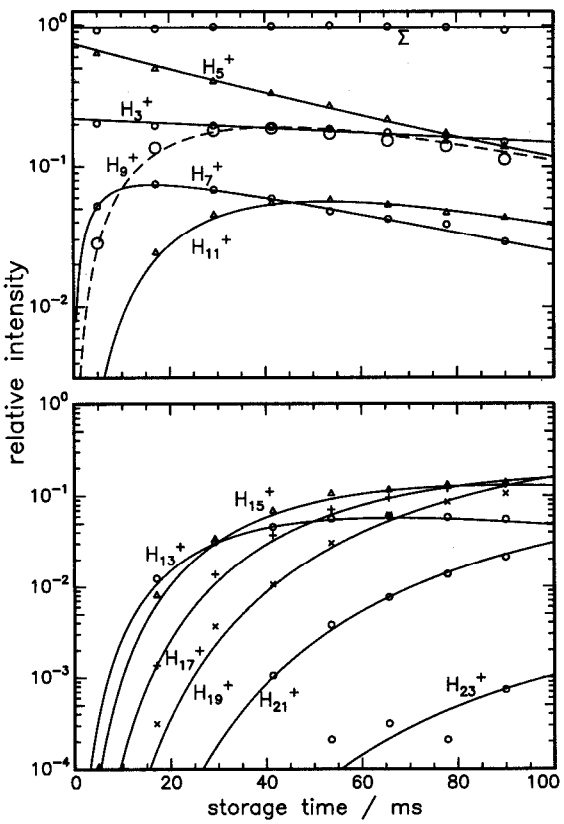

Fig. 5. Evolution of the trap contents after injection of H_5^+ into p-H_2 at a target gas number density of 8.10×10^{13} cm^{-3} and a temperature of 11 K. Symbols and lines as in Fig. 3. The specific role of H_9^+ (broken line) is discussed in the text.

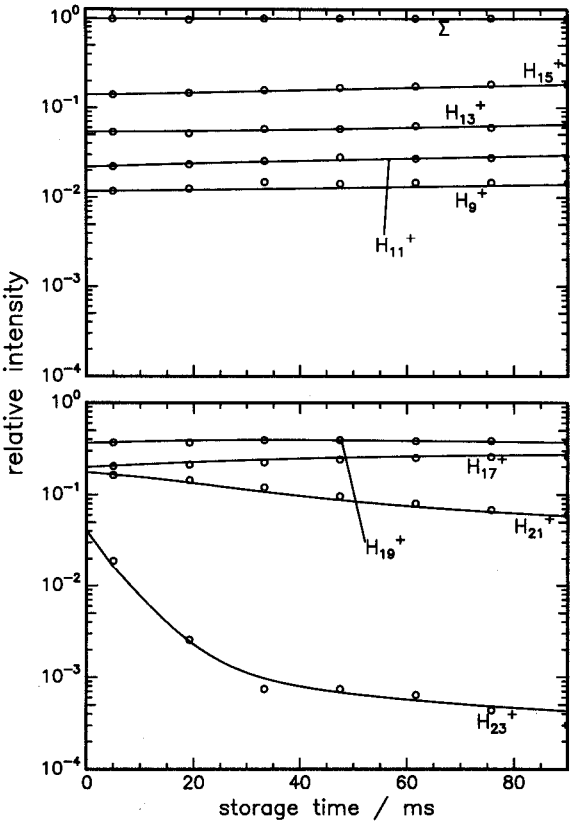

Fig. 6. Evolution of the trap contents after injection of H_{25}^+ into n-H_2 at a target gas number density of 3.80×10^{13} cm^{-3} at 10 K. The parent ions have disappeared before ion thermalization is finished. Fragmentation of H_{23}^+ is the dominant process. Symbols represent experimental data points and lines best fits according to the analysis described in the text.

H_{25}^+. Fragmentation for this large cluster appears to be a very rapid process and most of the initial clusters have disappeared into fragments before thermalization is completed. For that reason only the decay of H_{23}^+ is observable on the time scale of the plot. Equilibrium conditions are reached after less than 100 ms for all fragments appearing. Therefore these measurements focusing on the fragmentation are only sensitive to the dynamics of a few cluster sizes. Rate coefficients derived from these different measurements agree within experimental error with the values determined for smaller parent clusters, thus confirming validity of the experimental method and analysis employed in this study.

Ternary rate coefficients k_3 for clusters $H_3^+, \ldots, H_{23}^+$ and the corresponding fragmentation rates have ben extracted as described above at a nominal temperature of 10 K in reaction with normal and para hydrogen. Since for larger clusters the scatter of the effective binary rate coefficient k_g as a function of the hydrogen number density was significantly larger than for smaller clusters, we completely neglected radiative association and derived k_3 from the reaction time constants by dividing the reaction rates, $(1/\tau_g)$, by the square of the number density, $[H_2]$. Rate coefficients are compiled in Table 1 for ternary association (k_3) and in Table 2 for fragmentation rate

Table 1
Rate coefficients for ternary association, k_3, and calculated dissociation times, τ_{dis}, for the two hydrogen modifications, n-H_2 and p-H_2, as a function of cluster size H_i, $i = 3$–21. The numbers in parentheses are powers of 10

Cluster	k_3(n-H_2) ($cm^6\ s^{-1}$)	k_3 (p-H_2) ($cm^6\ s^{-1}$)	τ_{dis}(n-H_2) (ns)	τ_{dis} (p-H_2) (ns)
H_3^+	1.5 ± 0.5 (−28)	6.0 ± 2.0 (−28)	0.39	0.96
H_5^+	2.5 ± 0.5 (−28)	4.0 ± 1.0 (−27)	0.74	7.3
H_7^+	9.0 ± 3.0 (−28)	2.0 ± 1.0 (−26)	2.8	39.2
H_9^+	3.0 ± 1.0 (−27)	8.0 ± 2.0 (−27)	9.9	16.3
H_{11}^+	1.0 ± 0.5 (−26)	2.5 ± 1.5 (−26)	34.0	52.4
H_{13}^+	1.0 ± 0.5 (−26)	2.5 ± 1.5 (−26)	35.0	53.6
H_{15}^+	8.0 ± 5.0 (−27)	1.3 ± 0.5 (−26)	28.2	28.3
H_{17}^+	6.0 ± 3.0 (−27)	1.0 ± 0.5 (−26)	21.4	21.9
H_{19}^+	1.5 ± 0.7 (−27)	5.0 ± 3.0 (−27)	5.4	11.1
H_{21}^+	5.0 ± 4.0 (−28)	1.0 ± 0.5 (−27)	1.8	2.2

coefficients (k_f). In Figs. 7 and 8 these rate coefficients are plotted as a function of the step in the reaction chain ($i \rightarrow i+2$) and ($i \rightarrow i-2$) respectively.

For both target species, p-H_2 and n-H_2, k_3 peaks at the 11 → 13, 13 → 15 reaction steps whereas k_f has a plateau region ranging from sizes 11 to 19. For larger clusters fragmentation rate coefficients increase steeply. This overall finding is consistent with a broad equilibrium cluster size distribution around a maximum of about H_{19}^+ (see Fig. 2).

Up to date measurements of k_3 are only available for the first reaction step $H_3^+ \rightarrow H_5^+$ and at higher temperatures (see Table 3). Bates [33] and Herbst [34] predict that the thermal rate coefficient for ternary association $k_3(T)$ should vary as T^{-x} with $x \approx 2.5$ for this reaction. Results from Table 3 show a $1/T$ dependence and our present value at 10 K is consistent with this trend

Interestingly, not only ternary association but also binary fragmentation has a larger rate coefficient and therefore both processes proceed faster with para hydrogen for all cluster sizes. For the association of the smallest three clusters this difference is extraordinarily pronounced leading to a sharp drop in k_3 (p-H_2) from reaction step 7 → 9 to 9 → 11. This result has been pointed out above as the

Table 2
Binary rate coefficients for fragmentation, k_f, for the two hydrogen modifications, n-H_2 and p-H_2, as a function of cluster size H_i, $i = 5$–23

Cluster	k_f (n-H_2) ($cm^3\ s^{-1}$)	k_f (p-H_2) ($cm^3\ s^{-1}$)
H_5^+	5.0 ± 5.0 (−16)	5.0 ± 5.0 (−16)
H_7^+	5.0 ± 5.0 (−16)	5.0 ± 5.0 (−16)
H_9^+	2.0 ± 1.5 (−14)	8.0 ± 4.5 (−14)
H_{11}^+	2.0 ± 1.5 (−13)	5.0 ± 2.5 (−13)
H_{13}^+	5.0 ± 4.0 (−13)	1.3 ± 0.6 (−12)
H_{15}^+	3.5 ± 2.5 (−13)	1.1 ± 0.5 (−12)
H_{17}^+	5.0 ± 3.0 (−13)	1.0 ± 0.5 (−12)
H_{19}^+	5.0 ± 3.0 (−13)	1.3 ± 0.6 (−13)
H_{21}^+	5.0 ± 3.0 (−13)	0.9 ± 0.4 (−13)
H_{23}^+	1.5 ± 1.0 (−12)	2.4 ± 1.2 (−12)

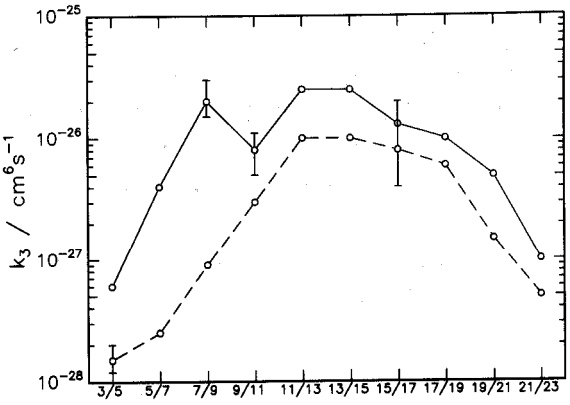

Fig. 7. Rate coefficients for the ternary association k_3 of hydrogen cluster ions ($H_i^+ \rightarrow H_{i+2}^+$) stored in n-$H_2$ (lower curve) and p-H_2 (upper curve) at a nominal temperature of 10 K. Typical error bars are given for several values and represent best fit results for 80% of all measurements.

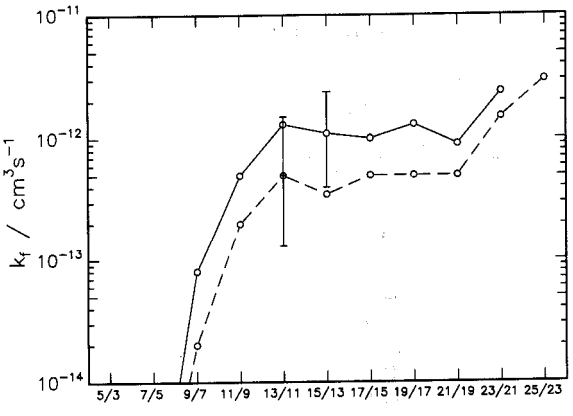

Fig. 8. Binary rate coefficients for the fragmentation k_f of hydrogen cluster ions ($H_i^+ \rightarrow H_{i-2}^+$) stored in n-$H_2$ (lower curve) and p-H_2 (upper curve) at a nominal temperature of 10 K. Values for the two first reaction steps 5/3 and 7/5 are out of range (see Table 2). Typical error bars are given for several values and represent best fit results for 80% of all measurements.

reaction step 9 → 11 being a bottleneck in the cluster formation chain. This is the most intriguing feature of the current measurements which together with the other findings yield some dynamical information that will be discussed in the following section.

4. Discussion

4.1. Dynamics

The time between two collisions, the elementary dynamical steps, is on the order of microseconds at the current target gas number densities. Internal processes within a cluster such as internal vibrational relaxation (IVR) and dissociation are happening on a much shorter time scale; τ_{IVR} (picosecond to nanosecond) and τ_{dis} (nanosecond) respectively.

Table 3
Ternary association rate coefficient in $cm^6\ s^{-1}$ for H_3^+ with normal hydrogen at different temperatures

T (K)	k_3 ($cm^6\ s^{-1}$)	Ref.
210	$4.6 \pm 0.5\ (-30)$	[23]
158	$1.2 \pm 3.0\ (-29)$	[23]
80	$2.5 \pm 0.7\ (-29)$	[24,25]
25	$7.0 \pm 3.0\ (-29)$	[25,37]
10	$1.5 \pm 0.5\ (-28)$	This work

This separation of the individual time scales allows us to describe the dynamics of clustering in a simple sequential step model for both growth and fragmentation of hydrogen cluster ions. For the latter the rate equation is given by Eq. (2) and the corresponding binary rate coefficient k_f is proportional to the bimolecular rate coefficient k_c:

$$k_f = f_{H_2} k_c \tag{5}$$

where f_{H_2} denotes the fraction of those collisions leading to fragmentation.

In the case of association the first step is the formation of an intermediate complex with a bimolecular rate coefficient which is also given by k_c:

$$H_i^+ + H_2 \xrightarrow{k_c} (H_{i+2}^+)^*$$

The second step is either unimolecular redissociation

$$(H_{i+2}^+)^* \xrightarrow{1/\tau_{dis}} H_i^+ + H_2$$

with a rate of $1/\tau_{dis}$ or stabilization via collision with another H_2 molecule:

$$(H_{i+2}^+)^* + H_2 \xrightarrow{1/\tau_{H_2}} (H_{i+2}^+) + H_2$$

The corresponding collision stabilization rate $1/\tau_{H_2}$ can be written as

$$1/\tau_{H_2} = k_c'[H_2] g_{H_2} \tag{6}$$

where $[H_2]$ is the target gas number density and k_c' is the rate coefficient for collisions of $(H_{i+2}^+)^*$ with H_2. The factor g_{H_2} represents the fraction of collisions that lead to stabilization.

Since $\tau_{dis} \ll \tau_{H_2}$, the fraction of stabilized product clusters is, to a good approximation, given by the ratio τ_{dis}/τ_{H_2}. The apparent second-order rate coefficient for association, k_g, can be calculated by multiplying this fraction by the rate coefficient for complex formation,

k_c, using Eq. (6):

$$k_g = \tau_{dis} \cdot g_{H_2} \cdot k_c k'_c [H_2] \quad (7)$$

with

$$\tau_{dis} \cdot g_{H_2} \cdot k_c k'_c = k_3 \quad (8)$$

Commonly used values for the stabilization efficiency g_{H_2} are in the range of 0.5–0.1 for molecular association reactions such as $C_2H_2^+ + 2H_2$ [30]. For the present study we assume for simplicity a constant value of 0.1 for all hydrogen clusters.

On the basis of the proposed reaction model, differences in the measured rate constants as a function of the cluster size as well as for the two nuclear spin species of hydrogen can be related to the three quantities k_c, τ_{dis} and g_{H_2}.

Considering the collision rate coefficients k_c and k'_c which enter in rate equations (5) and (8), one has to recall that at the energies of the present experiment the ion–H_2 capture cross-section is determined by the position of the centrifugal barriers of the long-range ion-induced dipole and quadrupole interaction (≥ 10 Å). This distance is much larger than the dimension of the cluster (e.g. for H_9^+ less than 3 Å). For this reason values of k_c are almost independent of cluster size. Only the reduced mass, which is mainly determined by the mass of the light H_2 target, leads to a slight decrease in the rate coefficients for larger clusters. Due to the anisotropy of the ion–H_2 potential the collision rate with the (non-rotating) para hydrogen molecule is large compared to that with ortho hydrogen. This difference between para and ortho hydrogen has been calculated on the basis of values derived from trajectory calculations using a suitable long-range interaction potential for the reaction $H^+ + o\text{-}H_2/p\text{-}H_2$ [35]. For reaction with n-H_2 at collision energies of 1 meV and below this ratio is $k_c(n\text{-}H_2) = 0.7\, k_c(p\text{-}H_2)$.

Experimental values of k_f ($\approx k_c$) and k_3 ($\approx k_c k'_c$) are larger for p-H_2 compared to n-H_2 for all cluster sizes. Ratios of the rate coefficients for both hydrogen species yield values which agree with the ratios $k_c(p\text{-}H_2)/k_c(n\text{-}H_2)$ and $[k_c(p\text{-}H_2)/k_c(n\text{-}H_2)]^2$ for fragmentation and association respectively. Therefore we conclude that the difference in k_c explains the overall trend of larger rate coefficients in collisions with para hydrogen except for the enormous difference in $k_3(p\text{-}H_2)$ versus $k_3(n\text{-}H_2)$ for the first three reaction steps.

The only other quantities entering into k_3 (Eq. (8)) are g_{H_2} and τ_{dis}. For the sake of simplicity we assume g_{H_2} to be constant and relate the major effect solely to τ_{dis}. As a result τ_{dis} shows the same trend as a function of cluster size as k_3 (see Fig. 7). Using the measured effective binary rate coefficients for growth k_g, as well as k_c and the estimate for g_{H_2}, τ_{dis} has been determined by solving Eq. (8). Resulting dissociation times are listed in Table 1 for both targets as a function of cluster size. These times are on the order of nanoseconds. Actual times might be somewhat shorter due to the assumption that $g_{H_2} = 0.1$ but this does not affect relative changes.

Based on the assumptions of the preceding discussion the unimolecular redissociation step determines whether a newly formed metastable cluster survives long enough to be stabilized. This process is strongly dependent on the total available energy (temperature) of the intermediate complex. In collisions with normal hydrogen this internal energy can be increased if o-H_2 transfers its rotational energy ($J = 1 \rightarrow 0, \Delta E_{rot} = 14.4$ meV) to the cluster. Since ortho–para conversion by direct nuclear spin flip in the approaching H_2 molecule is very unlikely, *scrambling* collisions are required for such a transition. Therefore the rotational energy only becomes available if a proton is exchanged between the cluster and the H_2 molecule or if the molecule breaks up and merges into the intermediate complex.

Because of the large differences in the derived dissociation times for the two hydrogen

modifications (see Table 1) we conclude that the rotational energy of ortho hydrogen is available to the complex at the reaction steps ($3 \rightarrow 5 \rightarrow 7 \rightarrow 9$). Therefore it must be concluded that *scrambling* is efficient in collisions of these small clusters ($i = 5$–7) with hydrogen. Complexes formed with p-H_2 are just *colder* and the corresponding dissociation times are longer by a factor of up to 20. The amount of rotational energy of o-H_2 is comparable to the total thermal energy available in the preceding cluster. The latter can be estimated by $(3i - 6)kT/2$, where i is the number of H atoms in the preceding cluster (e.g. for H_9^+, $E_{tot} \approx 10$ meV at 10 K). This energetic consideration shows that a large effect has to be expected at the low temperature of the present experiment if the rotational energy is available.

For larger clusters starting with H_9^+, τ_{dis} becomes comparable (Table 1) for both hydrogen targets. This indicates that transfer of rotational energy of o-H_2 to the cluster is much less efficient but not completely impossible as can be seen from the remaining differences in dissociation times for cluster sizes ($i = 9$–13). The further growth of H_{15}^+ seems to be independent of the rotational energy of the target, and therefore reaction is happening via *non-scrambling* collisions. This implies that H_2 stays intact as a distinguishable molecule and is loosely attached to a chemically bound core of H_9^+.

4.2. Binding energies

The present study of the dynamics of hydrogen cluster ions shows that the reaction mechanism is suitably characterized by the gain or loss of *one* H_2 molecule. The bond of the outer H_2 molecules is the shallowest potential well within the cluster. The breaking and forming of this bond are observed in our experiment. Therefore the bimolecular rate coefficient for fragmentation k_f, as well as the rate for redissociation after the formation of the intermediate complex $1/\tau_{dis}$ are measures for the strength of this bond. If we assume the energy dependence of the fragmentation cross-section to follow a threshold function proportional to $(E - \Delta E)^{1/2}$, where E is the collision energy and ΔE is the binding energy of the cluster of interest, we can write for the thermal rate coefficient of this process

$$k_f = k_c \exp\frac{-\Delta E}{kT} \tag{9}$$

where k_c is the capture rate coefficient and T the collision temperature. Using the measured k_f (Table 2) and the capture rate coefficient k_c, ΔE can be estimated from the above equation without any parameter or unknown to be considered. Values are in the range 11–9 meV (0.26–0.20 kcal mol^{-1}) for cluster sizes $i = 11$–21. It is noteworthy that our calculated ΔE values are smaller than the latest theoretical predictions by less than a factor of two for the larger clusters ($i = 11$–21). For a more precise estimate the internal energy of the cluster has also to be accounted for. This would lead to somewhat larger binding energies.

For the process of complex decay an expression similar to Eq. (9) for the reaction rate $1/\tau_{dis}$ can be found using simple statistical considerations. After the formation of the intermediate complex the bond energy is released and redistributed among all degrees of freedom of this new cluster. This IVR process is very fast compared to the redissociation step:

$\tau_{IVR} \ll \tau_{dis}$

The excess energy remains within the cluster for the time considered (τ_{dis}). It thus leads to an increase in the initial temperature T of this intermediate cluster. The rate for redissociation is proportional to the probability of reconcentrating the bond energy in the breaking bond at this elevated temperature T^* which may be written as

$$1/\tau_{dis} = \nu \exp\frac{-\Delta E}{kT^*} \tag{10}$$

Here ν is a rather arbitrary frequency (*vibration* along the fragmentation coordinate) and the exponential factor gives the ratio of success. The elevated temperature has been estimated by distributing the bond energy among all possible degrees of freedom in the cluster $(H_{i+2}^+)^*$, $(3(i+2)-6$, each with energy $kT^*/2)$. The unknown constant ν has been calculated from Eq. (10) using the derived value for τ_{dis} and adopting a recent ab initio value of ΔE for a given cluster size ($i = 15$) [36]. This constant ($\nu = 7 \times 10^{11}$ s^{-1}) has been used to determine ΔE as a function of cluster size. Bond energies within this simple statistical approach decrease from 28 to 11 meV (0.65 to 0.25 kcal mol^{-1}) as a function of cluster size $i = 11$–23), approaching the bulk limit of 9 meV. These values are larger by about a factor of two than the values derived from the rate of fragmentation.

Both estimates are significantly smaller than the values of Hiraoka [4] who has determined values in the range 75–26 meV for the same cluster size range. With binding energies as large as these one would expect the cluster size distribution at the low temperature of our experiment ($kT = 1.3$ meV) to extend to much larger masses than observed in the present study (see Fig. 2). In contrast, the steeply increasing fragmentation rates show that these clusters easily lose one hydrogen molecule under the conditions of the present investigation.

4.3. Structure

The hydrogen cluster ion is a complex system and in general measurements of rate coefficients do not reveal direct information on the structure of reactant or product clusters. However, the dynamical and energetic results of the present study allow for a principal classification of the structures of cluster ions. For smaller clusters ($i < 9$), colliding H_2 molecules lose their identity and their protons can be exchanged by protons of the preceding cluster. For larger clusters, approaching H_2 molecules remain as a peripheral unit in the new cluster. In addition, binding energies extracted from the present experiment for clusters in the range of $(11 < i < 23)$ approach the bulk limit, also indicating that the outer H_2 is bound to the cluster as a subunit. Therefore the first class of clusters has more the character of a molecular ion (H_i^+). Clusters of the second class consist of a molecular ion core (H_9^+) surrounded by more or less identical, loosely bound subunits (H_2). They may therefore be described as $H_9^+ \cdot (H_2)_n$.

Some support for this interpretation comes from the most recent theoretical studies of Farizon and co-workers [12,36]. The authors find most intramolecular distances to reach a constant value at a cluster size of H_9^+–H_{11}^+. Especially the H–H distance of pairs of the outer hydrogen atoms becomes very close to the free H_2 value. Moreover, H–H distances of the inner H_3^+ remain unchanged for larger clusters, showing that no strong interactions between outer hydrogen atoms and the core are present.

5. Conclusions

This experimental investigation represents the first study of the dynamics of growth and fragmentation of hydrogen cluster ions at low temperature. Dissociation of intermediately formed complexes $(H_{i+2}^+)^*$ turns out to be the process with the strongest size dependence. Therefore this reaction step determines how fast a cluster of specific size grows. A comparison of the results for para and normal hydrogen as a target reveals the existence of a dynamical shell structure, i.e. there seems to be no exchange between the H_9^+ core and additional hydrogen molecules. The possibility of particle exchange (*scrambling* collisions) can be tested by using isotopic tracers D_2 or HD

as a target for different parent clusters. Experiments along these lines are under way and will provide more insight into the dynamics and energetics of the hydrogen cluster ions. The effect of isotopic fractionation has already been observed in the mass spectra of the present study (see Fig. 2).

Large differences in the rate coefficient for ternary association, k_3, are apparent between p-H_2 and n-H_2 for small clusters. The fact that n-H_2 contains already 25% of p-H_2 raises the question whether clusters are formed in collisions with o-H_2. Preliminary measurements with different para contents have been carried out for the first three reaction steps. Fig. 9 shows the rate coefficient for ternary association as a result of eight series of measurements within the experimentally accessible range of para hydrogen contents ($x_{p\text{-}H_2}$), 0.25–1. The rate coefficient becomes very small for small p-H_2 contents. Therefore o-H_2 does not contribute significantly to the formation of hydrogen cluster ions. In addition, k_3 rises non-linearly as a function of the p-H_2 content. Even at p-H_2 concentrations as high as 80%, k_3 is only about 20% of the pure para hydrogen value. This preliminary finding indicates that for these small clusters *scrambling* might play a role not only in reactive but also in thermalizing collisions leading to a significant increase of the internal temperature of the parent cluster. Besides these energetic considerations this overall behavior of k_3 may also be related to angular momentum constraints, symmetry restrictions of this particular collision system, or to specific dynamical features such as the rotational averaging of the potential energy surface.

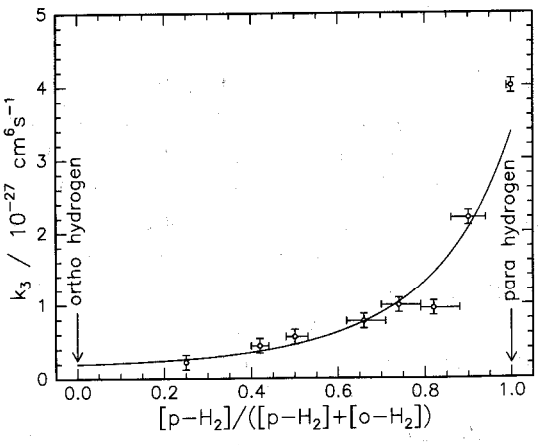

Fig. 9. Ternary association rate coefficient k_3 as a function of the p-H_2 content for H_5^+ at a nominal temperature of 10 K. Arrows indicate the limits of pure ortho and para hydrogen. The curve serves as a guide to the eye and illustrates that k_3 becomes very small in the ortho limit.

At present, only the long-range part of the potential, harmonic frequencies, and a few low lying stationary points are known for hydrogen cluster ions [12,36]. For a quantitative interpretation of the results of the present experimental study more information on the potential is needed. For an accurate statistical modeling of our low temperature experiments, anharmonicities and reliable zero-point energies are required. Potential barriers for the proton exchange are expected to explain the dynamics of *scrambling*.

Acknowledgments

We would like to thank M.J. Gaillard, M. Farizon and co-workers for providing us with the results of their calculations prior to publication. This work was supported by the Deutsche Forschungsgemeinschaft (SFB 276, Freiburg and INK 2, Chemnitz).

References

[1] P.H. Dawson and A.W. Tickner, J. Chem. Phys., 37 (1962) 672.
[2] R. Clampitt and L. Gowland, Nature, 223 (1969) 815.
[3] A. van Deursen and J. Reuss, Int. J. Mass Spectrom. Ion Phys., 11 (1973) 483.
[4] K. Hiraoka, J. Chem. Phys., 87 (1987) 4048.
[5] R. Ahlrichs, Theor. Chim. Acta, 39 (1975) 149.
[6] G.D. Carney, Mol. Phys., 39 (1980) 923.
[7] K. Hirao and S. Yamabe, Chem. Phys., 80 (1980) 237.
[8] Y. Yamaguchi, J.F. Gaw, R.B. Remington and H.F. Schaefer III, J. Chem. Phys., 86 (1987) 5072.

[9] N.J. Kirchner and M.T. Bowers, J. Phys. Chem., 92 (1987) 2573.
[10] S. Yamabe, K. Hirao and K. Kitaura, Chem. Phys. Lett., 56 (1978) 546.
[11] Y. Yamaguchi, J.F. Gaw and H.F. Schaefer III, J. Chem. Phys., 78 (1983) 4074.
[12] M. Farizon, H. Chermette and B. Farizon-Mazuy, J. Chem. Phys., 96 (1992) 1325.
[13] K. Hiraoka and P. Kebarle, J. Chem. Phys., 62 (1975) 2267.
[14] R. J. Beuhler, S. Ehrenson and L. Friedman, J. Chem. Phys., 79 (1983) 5982.
[15] M.T. Elford, J. Chem.Phys., 79 (1983) 5951.
[16] K. Hiraoka and T. Mori, Chem. Phys. Lett., 157 (1989) 467.
[17] M. Okumura, L. Yeh and Y.T. Lee, J. Chem. Phys., 88 (1988) 79.
[18] A. van Lumig and J. Reuss, Int. J. Mass Spectrom., Ion Phys., 27 (1978) 197.
[19] M. Chevallier, A. Clouvas, H.J. Frishkorn, M.J. Gaillard, J.C. Poizat and J. Remillieux, Z. Phys. D, 2 (1986) 87.
[20] S. Ouaskit, B. Farizon, M. Farizon, M.J. Gaillard and E. Gerlic, Phys. Rev. A, 49 (1994) 1484.
[21] S. Ouaskit, B. Farizon, M. Farizon, M.J. Gaillard, A. Chevarier, N. Chevarier, E. Gerlic and M. Stern, Int. J. Mass Spectrom. Ion Processes, 139 (1994) 141.
[22] B. Farizon, M. Farizon, M.J. Gaillard, E. Gerlic and S. Ouaskit, Z. Phys. D, 33 (1995) 53.
[23] R. Johnson, C. Huang and M. Biondi, J. Chem. Phys., 65 (1976) 1539.
[24] G.Kaefer, Ph.D. Thesis, Universität Freiburg, 1989.
[25] D. Gerlich, G. Kaefer and W. Paul, in T.D. Märk and F. Howorka (Eds.), Symposium on Atomic and Surface Physics, Obertraun, 1990, p. 332.
[26] E. Teloy and D. Gerlich, Chem. Phys., 4 (1974) 417.
[27] D. Gerlich, Adv. Chem. Phys., LXXXII (1992) 1.
[28] G. Miller, J. Phys. Chem., 67 (1963) 1359.
[29] W. Paul and D. Gerlich, in T. Anderson, B. Fastrup, F. Folkmann and H. Knudsen (Eds.), ICPEAC Book of Contributed Papers, Aarhus University, Aarhus, 1993, p. 807.
[30] D. Gerlich and S. Horning, Chem. Rev., 92 (1992) 1509.
[31] D. Gerlich, in I. Nenner (Ed.), Molecules and Grains in Space, AIP Press, New York, 1994, p. 489.
[32] W.H. Press, R.P. Flamery, S.A. Tenkolsky and W.T. Vetterling, 2nd edn., Numerical Recipes in C, Cambridge University Press, 1990.
[33] D.R. Bates, J. Phys. B, 12 (1979) 4135.
[34] E. Herbst, J. Chem. Phys., 70 (1979) 2201.
[35] D. Gerlich, J. Chem. Phys., 92 (1990) 2377.
[36] B. Farizon, M. Farizon, H. Chermette and M.J. Gaillard, J. Chem. Phys., submitted for publication.
[37] W. Paul, Diplom Thesis, Universität Freiburg, 1990.